Int J Fract (2010) 161:161–173
DOI 10.1007/s10704-010-9450-4

ORIGINAL PAPER

An integrated cohesive/overlapping crack model for the analysis of flexural cracking and crushing in RC beams

Alberto Carpinteri · Mauro Corrado · Marco Paggi

Received: 30 July 2009 / Accepted: 14 January 2010 / Published online: 7 February 2010

Abstract In the present paper, a new fracture-mechanics based model is proposed for the analysis of reinforced concrete beams in bending describing both cracking and crushing growths taking place during the loading process by means of the concept of strain localization. In particular, the nonlinear behaviour of concrete in compression is modelled by the *Overlapping Crack Model*, which considers a material interpenetration when the elastic limit is overcome, in close analogy with the *Cohesive Crack Model*, routinely adopted for modelling the tensile behaviour of concrete. On the basis of different nonlinear contributions due to concrete and steel, a numerical finite element algorithm is proposed. According to this approach, the flexural behaviour of reinforced concrete structural elements is analyzed by varying the main geometrical and mechanical parameters. Particular regard is given to the role of the size-scale effects on the ductility of plastic hinges, which is available at the ultimate load conditions.

Keywords Reinforced concrete · Cohesive Crack Model · Nonlinear analysis · Finite element method · Crushing · Ductility · Overlapping Crack Model

A. Carpinteri · M. Corrado (✉) · M. Paggi
Department of Structural Engineering and Geotechnics, Politecnico di Torino, Corso Duca degli Abruzzi 24, 10129 Torino, Italy
e-mail: mauro.corrado@polito.it

1 Introduction

Structural ductility is a fundamental property for the safe design of reinforced concrete (RC) structures. From a practical point of view, this requirement is satisfied by complying with some empirical prescriptions provided by the existing design codes. In the case of RC elements, in fact, an accurate evaluation of the available ductility is difficult to be achieved due to the simultaneous presence of several nonlinear contributions affecting the global mechanical behaviour, such as concrete cracking in tension, steel yielding or slippage, and concrete crushing in compression. It is worth noting that, among the various forms of nonlinearity, concrete crushing, which highly depends on the size-scale of the specimen, is fundamental for the prediction of the ultimate rotation, since it delimits the plastic plateau of the moment versus rotation diagrams.

In structural design, the concrete contribution in tension is usually totally neglected or just considered with a linear-elastic stress–strain law until the ultimate tensile strength is reached. A more accurate description of the nonlinear behaviour of concrete has been provided in the framework of the finite element method (see Owen and Hinton 1980 for a wide overview on computational aspects), where several models based on plasticity (Pramono and Willam 1989; Owen et al. 1983; De Borst 1986) or on a combination of damage and plasticity (Simo and Ju 1987; Grassl and Jiràsek 2006) have been proposed. However, as pointed out by Morley (2008), the application of plasticity

theories does not allow the study of size-scale effects, in spite of their apparently successful applications over a wide range of structures of ordinary size. More recent research trends show the integration of plasticity with fracture mechanics theories, such as the smeared crack model (Cervenka and Papanikolaou 2008), in order to capture size-scale effects due to concrete cracking.

As far as the nonlinear constitutive behaviour of concrete in compression is concerned, it can be traditionally modelled in the framework of elasto-plasticity (Barbosa and Ribeiro 1998). A hardening/softening plasticity model based on the Menétrey and Willam (1995) three-parameter failure surface was used to simulate concrete crushing. Papanikolaou and Kappos (2007) proposed a plasticity formulation for multiaxial compression handling confinements effects. Alternatively, the local behaviour of the material can be governed by the Drucker–Prager yield criterion. The linear elastic behaviour governs the analysis until exceeding the compressive strength. Once the principal stress reaches the compressive strength, crushing takes place and the crushed regions develop perpendicular to the direction of principal stress. To model this nonlinear process, iterative algorithms with high performance computers have to be used. The main drawback of such an approach is represented by the fact that the parameters defining the yield surface have to be updated during the loading process in order to capture the softening response of the material. This was shown by Cela (2002), who proposed a material identification procedure for modelling the uniaxial compression tests of concrete. The extension of such an approach to bending specimens is still an open point. With regard to the steel behaviour, the most used constitutive laws are the elastic-perfectly plastic or the elastic-hardening stress–strain relationships.

A completely different approach can be pursued by applying fracture mechanics concepts to modelling crack growth and crushing processes. The *Bridged Crack Model*, for instance, has been largely used to study the mechanical stability of under-reinforced concrete beams and fibre reinforced structural elements (Carpinteri 1984; Carpinteri and Massabò 1997; Carpinteri et al. 2004). Recent applications permit to predict the mutual transitions between the different collapse mechanisms—flexural, shear or crushing failures—by varying the governing parameters (Carpinteri et al. 2007a). However, such a model is not able to fully describe the crushing process, which strongly influences the ultimate condition, making impossible the evaluation of the structural ductility. In this paper, in order to overcome this drawback, a different approach, still based on nonlinear fracture mechanics models, is proposed. In particular, the tensile cracking phenomenon is described by means of the well established *Cohesive Crack Model*, whereas the crushing process is modelled according to the *Overlapping Crack Model*, which considers a material interpenetration in the post-peak regime (Carpinteri et al. 2007b). As far as RC beams in bending are concerned, in fact, the crushing process may lead either to material expulsion to the upper side or to fragmentation. This is therefore the result of a severe strain localization which is analogous to what happens in uniaxial compression. Hence, the use of a fictitious interpenetration instead of a strain is fully justified by the fact that energy dissipation in compression takes place over a surface, rather than within a volume. Although this interpenetration in compression can be considered as an artefact introduced for modelling purposes, it permits to describe in a simplified way the actual failure mode. In fact, the results by Jansen and Shah (1997) show that, regardless of the failure mode of concrete specimen in uniaxial compression tests, the concept of overlapping crack can be profitably applied to predict the mechanical response even when inclined shear bands develop. In the present paper, this concept is generalized to the analysis of the behaviour of RC beams in bending. In this field, most of the available models require a detailed description of the triangular-shaped wedge which is expelled during crushing (e.g., Fantilli et al. 2007). With respect to such approaches, the proposed model permits to avoid the elaborate description of the kinematics of the failure mode.

Consequently, the analysis of the mechanical behaviour of RC structural elements will be carried out by means of a complex algorithm obtained by merging the two aforementioned elementary fracture mechanics models, along with a suitable constitutive law for steel. Diagonal shear cracks are not considered in the present work. With this algorithm, based on the finite element method, we will show that it is possible to completely capture the moment versus rotation response under monotonic loadings, taking into account all the main nonlinear contributions. A parametric analysis will provide a detailed quantification of the effect of the most important parameters entering the proposed model on the ductility of RC beams in bending, with

special regard on size-scale effects. A wide experimental comparison will show the effectiveness of the proposed approach.

2 Mathematical formulation

Let us consider a portion of a RC beam subjected to a bending moment M. This element, having a span to depth ratio equal to unity, is representative of the zone where a plastic hinge formation takes place. We also assume that fracturing and crushing processes are fully localized along the mid-span cross-section of this element. This assumption, fully consistent with the crushing phenomenon, also implies that only one equivalent main tensile crack is considered.

2.1 Cohesive Crack Model

In the proposed algorithm, the behaviour of concrete in tension is described by means of the well established Cohesive Crack Model (Hillerborg et al. 1976; Carpinteri 1985, 1989), largely used, in the past, to study the ductile-to-brittle transition in the mechanical response of plain concrete beams in bending. According to this model, the constitutive law for the undamaged zone is a $\sigma - \varepsilon$ linear-elastic relationship up to the achievement of the tensile strength, σ_u (Fig. 1a). In the process zone, the damaged material is still able to transfer a tensile stress across the crack surfaces. The cohesive stresses are considered to be linear decreasing functions of the crack opening, w^t (see Fig. 1b):

$$\sigma = \sigma_u \left(1 - \frac{w^t}{w^t_{cr}}\right), \tag{1}$$

where w^t_{cr} is the critical value of the crack opening corresponding to $\sigma = 0$, and σ_u is the ultimate tensile strength of concrete. The area under the stress versus displacement curve in Fig. 1b represents the fracture energy, $\mathcal{G}_F$, which ranges from 0.050 to 0.150 N/mm for concrete.

2.2 Overlapping Crack Model

In order to model the concrete crushing failure, the Overlapping Crack Model is adopted (Carpinteri et al. 2007b). Based on the original insights provided by

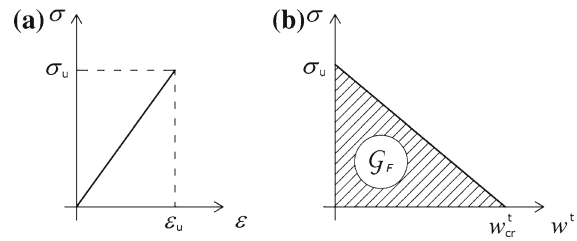

Fig. 1 *Cohesive Crack Model* for concrete in tension: linear-elastic $\sigma - \varepsilon$ law (**a**); post-peak softening $\sigma - \varepsilon$ relationship (**b**)

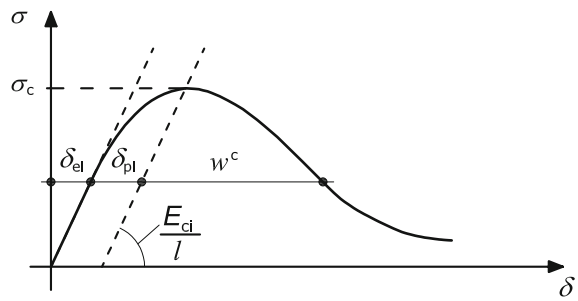

Fig. 2 Evaluation of the localized interpenetration, w^c, from the total shortening of the specimen, δ

Kotsovos (1983), van Mier (1984) and Jansen and Shah (1997), the interpenetration w^c is computed by subtracting the elastic elongation, caused by the reduction of the applied stress in the post-peak regime, δ_{el}, and the pre-peak plastic deformation, δ_{pl}, from the $\sigma - \delta$ diagram (see Fig. 2).

Typical stress-interpenetration curves obtained from specimens with different size and slenderness are shown in Fig. 3 (see also Carpinteri et al. (2010) for a comprehensive analysis of these curves for quasi-brittle materials). The collapse of the different curves onto a very narrow band proves the size-scale and slenderness independences of the overlapping crack law. Although this is nonlinear, the use of a simplified linear softening expression is considered for modelling purposes (see the dashed line in Fig. 3 for a visual comparison). This is a reasonable approximation because only the range $0.0 < w^c/w^c_{cr} < 0.5$ is usually utilized in the numerical simulations of RC beams in bending.

According to this assumption, in fact, the Overlapping Crack Model permits to describe in a simplified way the actual failure mode that can be very complex and may range from shear crack propagation to concrete fragmentation (RILEM TC 148-SSC 1997; Carpinteri et al. 2001). Hence, this concept permits

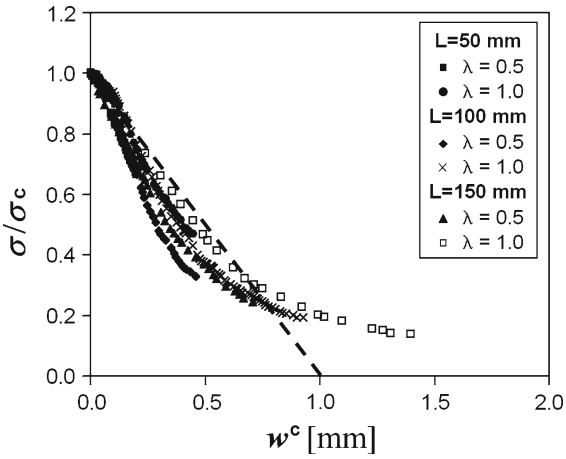

Fig. 3 Experimental and linear-softening approximation (*dashed curve*) for uniaxially compressed concrete specimens with different sizes and slendernesses

to avoid the elaborate description of the kinematics of these failure modes (Carpinteri et al. 2009). As a result, a pair of constitutive laws for concrete in compression is introduced, in close analogy with the Cohesive Crack Model: a stress–strain relationship until the compressive strength is achieved, and a stress–displacement (*overlapping*) relationship describing the phenomenon of concrete crushing (see the dashed line in Fig. 3). The latter law describes how the stress in the damaged material decreases from its maximum value to zero as the interpenetration increases from zero to the critical value, w_{cr}^{c}:

$$\sigma = \sigma_c \left(1 - \frac{w^c}{w_{cr}^c}\right), \tag{2}$$

where $w^c$is the interpenetration, w_{cr}^{c} is the critical value of the interpenetration corresponding to $\sigma = 0$ in the linear softening approximation, and σ_c is the compressive strength. It is worth noting that the crushing energy, $\mathcal{G}_C$, defined as the area below the post-peak softening curve of the dashed line in Fig. 3, can be considered as a material property, since it is not affected by the structural size. This is in full agreement with the recent fractal analyses by Ferro and Carpinteri (2008) and Carpinteri and Corrado (2009). The following empirical equation for calculating the crushing energy has recently been proposed by Suzuki et al. (2006), taking into account the confined concrete compressive strength by means of the stirrups yield strength and the stirrups volumetric content:

$$\mathcal{G}_C = \mathcal{G}_{C,0} + 10{,}000\frac{k_a^2 p_e}{\sigma_c}, \tag{3}$$

where σ_c is the average concrete compressive strength, $\mathcal{G}_{C,0}$ is the crushing energy for unconfined concrete:

$$\mathcal{G}_{C,0} = 80 - 50k_b, \tag{4}$$

k_a is a parameter depending on the stirrups strength and volumetric content:

$$k_a = 1 + k_e\frac{(f_{sy} - f_{s,c})}{f_{sy}}, \tag{5}$$

and p_e is the effective lateral pressure:

$$p_e = k_e\rho_w f_{s,c}. \tag{6}$$

The parameter k_b depends on the concrete compressive strength:

$$k_b = \frac{40}{\sigma_c} \leq 1.0, \tag{7}$$

$f_{s,c}$ is the stress in transverse reinforcement at the peak strength:

$$f_{s,c} = E_s\left[0.45\varepsilon_{c0} + 6.8\left(\frac{k_e\rho_w}{\sigma_c}\right)^{9/10}\right] \leq f_{sy}, \tag{8}$$

k_e is the effective confinement coefficient:

$$k_e = \left(1 - \sum\frac{(w_i')^2}{6b_c d_c}\right)\left(1 - \frac{s'}{2b_c}\right)\left(1 - \frac{s'}{2d_c}\right)/(1 - \rho_{cc}), \tag{9}$$

ρ_w is the geometric ratio of transverse reinforcement, E_s is the modulus of elasticity of transverse steel, $\varepsilon_{c0} = (0.0028 - 0.0008k_b)$, f_{sy} is the steel yield strength, w_i' is the spacing between longitudinal steel bars, s' is the spacing between stirrups, b_c and d_c are the widths of the concrete compressed zone, and ρ_{cc} is the longitudinal reinforcement ratio in the compression side. The units of measure in Eqs. (3)–(9) are N and mm.

By varying the concrete compressive strength from 20 to 90 MPa, Eq. (4) gives a crushing energy ranging from 30 to 58 N/mm. It is worth noting that $\mathcal{G}_C$ is between two and three orders of magnitude higher than $\mathcal{G}_F$. The crushing energy, in fact, may be interpreted as the sum of the fracture energy dissipated by the tensile microcracks taking place during the crushing phenomenon and the frictional energy. Typical critical values for crushing interpenetration and crack opening for normal strength concrete are approximately equal to $w_{cr}^{c} \approx 1$ mm (see also Jansen and Shah 1997) and $w_{cr}^{t} \approx 0.1$ mm, respectively. Finally, we remark that, in

the case of concrete confinement, the crushing energy, computed using Eq. (3), and the corresponding critical value for crushing interpenetration, considerably increase.

2.3 Steel–concrete interaction

In the proposed model, it is not possible to adopt the classical $\sigma - \varepsilon$ laws for steel, since the kinematics of the mid-span cross-section of the RC member is described by means of displacements, instead of strains. Consequently, a constitutive relationship between the reinforcement reaction and the crack opening displacement has to be introduced. In the past, this problem has been overcome by assuming a rigid-plastic behaviour for steel (Bosco and Carpinteri 1991). This assumption involves that the crack opening is zero up to steel yielding. Then, the reinforcement reaction is constant. In the proposed model, an approach closer to the actual behaviour is adopted, following the procedure proposed by Ruiz et al. (1999). The typical slip between reinforcing bar and surrounding concrete, in fact, allows for a crack opening before steel yielding. This phenomenon is taken into account by considering the relationship between the tangential stress along the steel–concrete interface and the relative tangential displacement, as proposed in Model Code 90 (Comité Euro-International du Béton 1993). By imposing equilibrium and compatibility conditions, it is possible to correlate the reinforcement reaction, given by the integration of the bond stresses acting along the bar, to the relative slip at the crack edge, which corresponds to half the crack opening displacement. Typically, the obtained relationship is characterized by an ascending branch up to steel yielding, after which the reaction is nearly constant. In this way, the actual bond-slip shear stress distribution is replaced by a pair of concentrated forces acting along the crack faces, functions of the opening displacement at the reinforcement level.

3 Numerical algorithm

A discrete form of the elastic equations governing the mechanical response of the two half-beams is herein introduced. The mid-span cross-section of the beam can be subdivided into finite elements by n nodes (Fig. 4a). In this scheme, cohesive and overlapping stresses are replaced by equivalent nodal forces, F_i, by integrating the corresponding tensile stresses over each element size. Such nodal forces depend on the nodal opening or closing displacements according to the cohesive or overlapping softening laws previously introduced.

The horizontal forces, F_i, acting at the i-th node along the mid-span cross-section can be computed as follows:

$$\{F\} = [K_\mathrm{w}]\{w\} + \{K_M\}\, M \tag{10}$$

where $\{F\}$ is the vector of nodal forces, $[K_\mathrm{w}]$ is the matrix of the coefficients of influence for the nodal displacements, $\{w\}$ is the vector of nodal displacements, $\{K_M\}$ is the vector of the coefficients of influence for the applied moment M.

In the generic situation shown in Fig. 4b, the following equations can be considered:

$$F_\mathrm{i} = 0; \quad \text{for i} = 1, 2, \ldots, (j-1)\,; \ \mathrm{i} \neq r \tag{11a}$$

$$F_\mathrm{i} = F_\mathrm{u}\left(1 - \frac{w_\mathrm{i}^\mathrm{t}}{w_\mathrm{cr}^\mathrm{t}}\right); \ \text{for i} = j, \ldots, (m-1)\,; \ \mathrm{i} \neq r \tag{11b}$$

$$w_\mathrm{i} = 0; \quad \text{for i} = m, \ldots, p \tag{11c}$$

$$F_\mathrm{i} = F_\mathrm{c}\left(1 - \frac{w_\mathrm{i}^\mathrm{c}}{w_\mathrm{cr}^\mathrm{c}}\right); \quad \text{for i} = (p+1), \ldots, n \tag{11d}$$

$$F_\mathrm{r} = f\,(w_\mathrm{r})\,; \quad \text{for i} = r. \tag{11e}$$

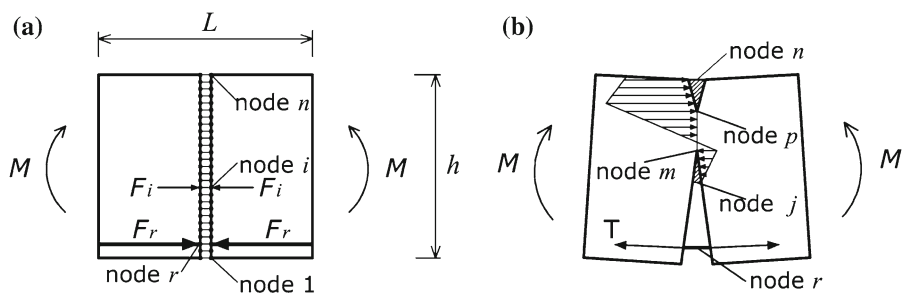

Fig. 4 Finite element nodes (**a**), and force distribution with cohesive crack in tension and crushing in compression (**b**) along the mid-span cross-section

where: j represents the real crack tip, m represents the fictitious crack tip, p is the fictitious overlapping tip and r is the node corresponding to the steel reinforcement. A bi-linear softening cohesive crack law can be easily introduced by modifying Eq. (11b). The reinforcement contribution is included in the nodal force corresponding to the r-th node (see Eq. (11e)). It is worth noting that, in this framework, it is possible to insert a reinforcement in compression by introducing another stress–displacement constitutive law in the corresponding node. Due to lack of studies on the behaviour of reinforcing bars in compression, the $\sigma - w$ relationship adopted is the same as that used for steel in tension.

Equations (10) and (11) constitute a linear algebraic system of $(2n)$ equations in $(2n+1)$ unknowns, namely $\{F\}$, $\{w\}$ and M. A possible additional equation can be chosen: we can set either the force in the fictitious crack tip, m, equal to the ultimate tensile force, or the force in the fictitious crushing tip, p, equal to the ultimate compression force. In the numerical scheme, we choose the situation which is closer to one of these two possible critical conditions. This criterion will ensure the uniqueness of the solution on the basis of physical arguments. The driving parameter of the process is the tip that in the considered step has reached the limit resistance. Only this tip is moved when passing to the next step.

It is important to remark that the present problem is nonlinear even if linear softening laws in tension and compression are considered. At each loading step, in fact, the size of the fictitious process zones in tension and in compression are unknown and have to be found iteratively. Therefore, the proposed numerical scheme is general and does not depend on the shape of the cohesive and overlapping crack laws being considered.

The two fictitious tips advance until they converge to the same node. So forth, in order to describe the descending branch of the moment-rotation diagram, the two tips can move together towards the intrados of the beam. As a consequence, the crack in tension closes and the overlapping zone is allowed to extend towards the intrados. This situation is quite commonly observed in over-reinforced beams, where steel yielding does not take place.

Finally, at each step of the algorithm, it is possible to calculate the localised rotation, ϑ, as follows:

$$\vartheta = \{D_{\mathrm{w}}\}^T \{w\} + D_M M \tag{12}$$

where $\{D_{\mathrm{w}}\}$ is the vector of the coefficients of influence for the nodal displacements and D_M is the coefficient of influence for the applied moment.

A feature of the proposed model is that it is unnecessary to introduce any assumptions on the deformation field as, for instance, the Bernoulli hypothesis. On the contrary, the longitudinal nodal displacements along the mid-span cross-section obtained through the step-by-step numerical solution are nonlinear. The nodal displacement profiles, in the case of a beam depth equal to 0.4 m and for an amount of tensile reinforcement equal to 2%, are shown in Fig. 5a, for different values of the applied bending moment. For low values of the bending moment, up to approximately 60% of the yielding value, the mechanical behaviour is characterized by a progressive advancing and opening of the tensile crack (see the crack tip position corresponding to $w = 0$). Concrete crushing starts developing just before the yielding moment and it becomes more and more evident by approaching the ultimate moment, when the nodal positions of the fictitious crack and overlapping tips coincide. The corresponding stress distributions along the mid-span cross-section are plotted in Fig. 5b.

3.1 Computation of the elastic coefficients

Equation (10) permits to analyse the fracturing and crushing processes of the mid-span cross-section taking into account the elastic behaviour of the RC member. To this aim, all the coefficients are computed *a priori* using a finite element analysis. In the present work, the FE code FEAP, developed by Prof. R. Taylor at the University of California, Berkeley, has been used. Due to the symmetry of the problem, a homogeneous concrete rectangular region, corresponding to half the tested specimen shown in Fig. 4a, is discretized by means of quadrilateral plane stress elements with uniform nodal spacing. Horizontal constraints are then applied to the nodes along the vertical symmetry edge. The coefficients $K_{\mathrm{w}}^{\mathrm{i,j}}$ entering Eq. (10), which relate the nodal force F_{j} to the nodal displacement w_{i}, have the physical dimensions of a stiffness and are computed by imposing a unitary horizontal displacement to each of the constrained nodes. On the other hand, by applying a unitary external bending moment, it is possible to compute the coefficients K_M^{i}. They have the physical dimensions of $[\mathrm{L}]^{-1}$. At the same time, each coefficient of influence for the nodal displacement on the global rotation, $D_{\mathrm{w}}^{\mathrm{i}}$,

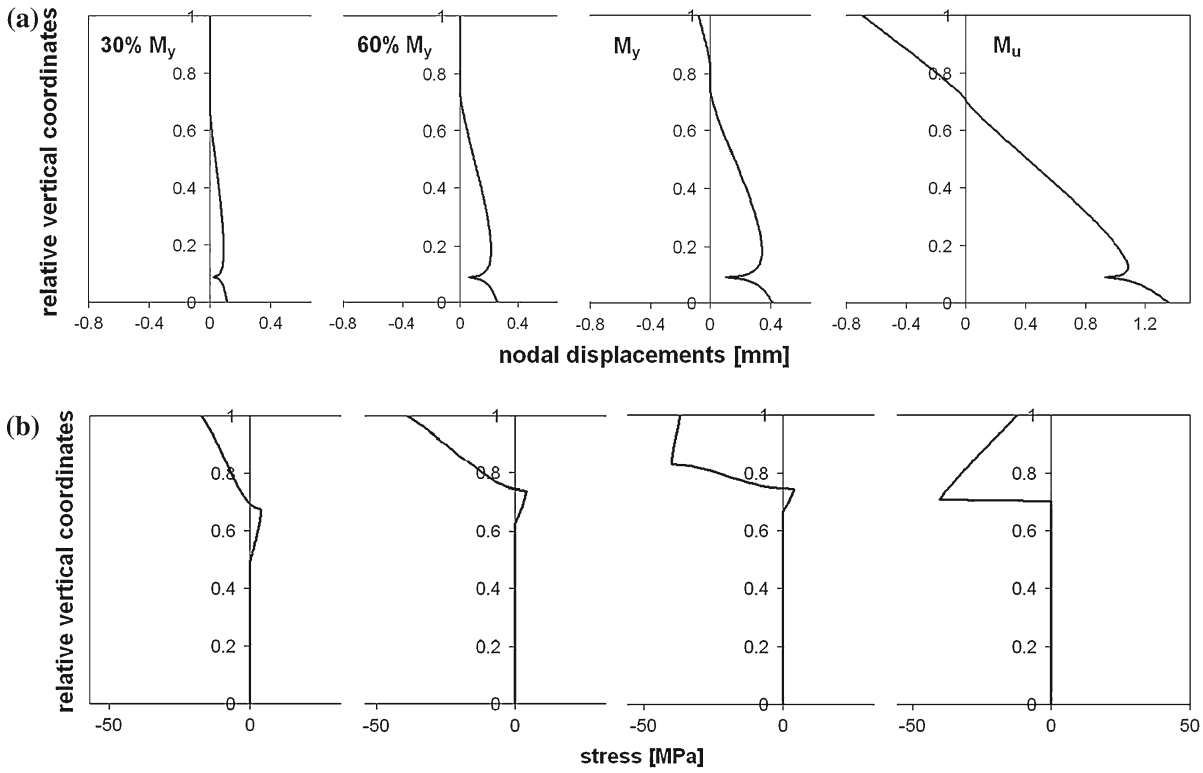

Fig. 5 Nodal displacement profiles (**a**), and concrete stress distributions (**b**) at different applied moments for $h = 0.4$ m and $\rho_t = 2\%$

entering Eq. (12), is given by the rotation of the free edge corresponding to a unitary displacement of the i-th constrained node and it has the physical dimensions of $[\mathrm{L}]^{-1}$. Finally, D_M is the rotation of the free edge corresponding to a unitary external bending moment and it has the physical dimensions of $[\mathrm{F}]^{-1}[\mathrm{L}]^{-1}$.

As regards the analysis of size-scale effects, the coefficients entering Eqs. (10) and (12) are connected by a simple relation of proportionality to the structural dimension. This means that it is not necessary to repeat the finite element analysis for any different considered beam size. More precisely, if all the three specimen sizes (depth h, span L, thickness b) are multiplied by a factor k, then the coefficients are transformed as follows:

$$K_{\mathrm{w}}^{\mathrm{i,j}}(kd) = kK_{\mathrm{w}}^{\mathrm{i,j}}(d), \tag{13a}$$

$$K_{M}^{\mathrm{i}}(kd) = \frac{1}{k}K_{M}^{\mathrm{i}}(d), \tag{13b}$$

$$D_{\mathrm{w}}^{\mathrm{i}}(kd) = \frac{1}{k}D_{\mathrm{w}}^{\mathrm{i}}(d), \tag{13c}$$

$$D_{M}(kd) = \frac{1}{k^3}D_{M}(d). \tag{13d}$$

On the other hand, if only depth and span are multiplied by the factor k, the thickness being kept constant, then Eqs. (13a,13d) are modified as follows:

$$K_{\mathrm{w}}^{\mathrm{i,j}}(kd) = K_{\mathrm{w}}^{\mathrm{i,j}}(d), \tag{14a}$$

$$D_{M}(kd) = \frac{1}{k^2}D_{M}(d), \tag{14b}$$

while Eqs. (13b, c) are unchanged.

4 Parametric analysis and experimental comparison

In this section, a parametric analysis is carried out to investigate on the influence of the main parameters affecting the global mechanical behaviour of RC beams in bending, namely the beam size, h, the tensile and compression steel percentages, ρ_t and ρ_c, the concrete compressive strength, σ_c, and the stirrups percentage, ρ_w. The percentages ρ_t, ρ_c and ρ_w are defined

as the ratios between the steel area and the beam cross-section area contained in the plane perpendicular to steel.

The slenderness, λ, and the thickness, b, are kept constant in the following examples and equal, respectively, to 1 and 0.2 m. The tensile yield strength of steel, σ_y, is set equal to 400 MPa. Moreover, detailed numerical–experimental comparisons are proposed on the basis of the results found in the Literature. The labels used to identify the different experimental curves coincide with those reported in the original papers.

4.1 Size-scale effects

The available ductility, measured by means of the rotation at failure, progressively decreases by increasing the beam size. In the case of high tensile steel percentage, as, e.g., $\rho_t = 2\%$, the typical trend obtained by varying the beam depth is shown in Fig. 6. Similar trends have been noticed for the other values of ρ_t. A plateau is observed in the nondimensional bending moment versus rotation diagram when steel yielding occurs. These curves put into evidence that the beam rotation at failure is progressively diminished by increasing the beam depth, with the appearance of sharper and sharper snap-back branches.

Such a trend is confirmed by the experimental evidences obtained by Corley (1966), Bosco and Debernardi (1993) and Bigaj and Walraven (1993). In particular, a close numerical–experimental comparison

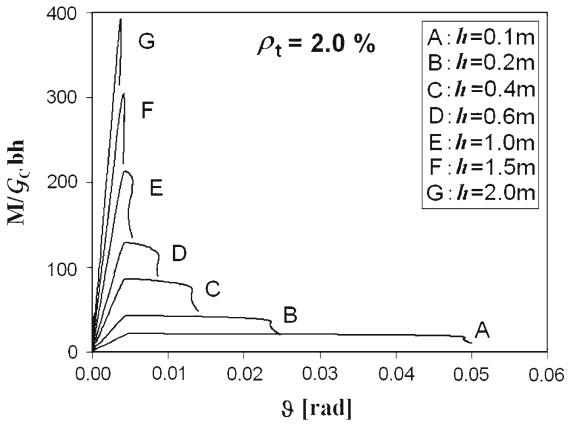

Fig. 6 Moment versus rotation diagrams for different beam depths, h

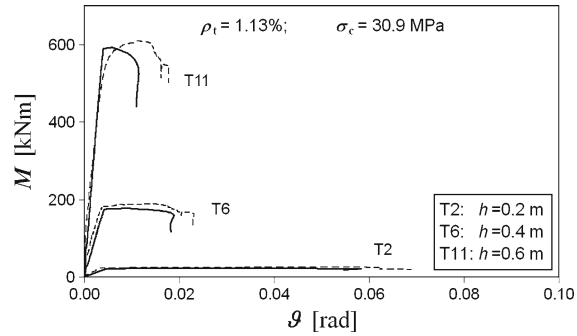

Fig. 7 Effect of the size of the tested beams: numerical (*solid lines*) versus experimental (*dashed lines*) moment-rotation curves. The experimental data are from Bosco and Debernardi (1993)

is shown in Fig. 7. The experimental data are from Bosco and Debernardi (1993).

4.2 Effect of the tensile steel reinforcement

In order to analyse the effect of the tensile steel percentage on the ductility, numerical simulations have been carried out by varying such a parameter, all the other geometrical and mechanical parameters being kept constant. The moment versus rotation curves for h=0.4 m, $\sigma_c = 40$ MPa, $\mathcal{G}_C = 30$ N/mm, $\sigma_u = 4$ MPa and $\mathcal{G}_F = 0.08$ N/mm are shown in Fig. 8a. The ultimate rotation increases by increasing the tensile reinforcement from 0.1 up to 0.5%, and it decreases subsequently. This result is in good agreement with the prescriptions of design codes (Comité Euro-International du Béton 1993), where a similar trend is proposed in terms of plastic rotation versus relative neutral axis depth (which is directly related to the amount of tensile reinforcement).

As a general remark, it is possible to state that the effect of the shape of the cohesive crack law is not of primary importance when the stress field is characterized by a strong gradient, as analytically and numerically shown in (Williams and Hadavinia 2002; Carpinteri et al. 2008) for double cantilever beam tests. Moreover, the examples proposed in this section focus on the evaluation of the post-peak branch of the moment-rotation curve, where the nonlinearity due to crushing and steel yielding or slippage are highly prevailing. The shape of the cohesive crack law influences the relative maximum of the ascending branch of the moment-rotation diagram before steel yielding or slippage (see

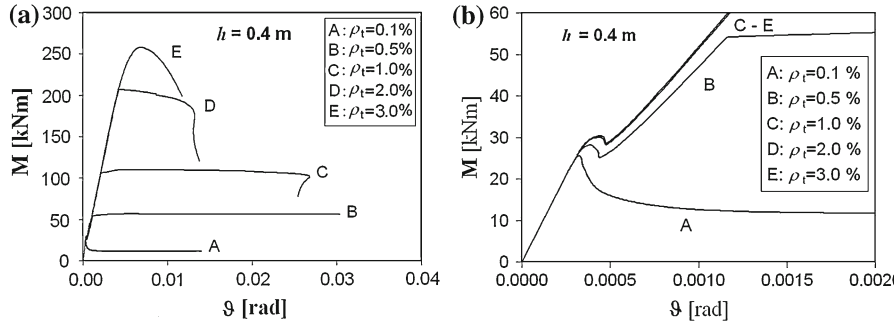

Fig. 8 Moment versus rotation diagrams for different tensile reinforcement percentages, ρ_t (**a**), and their magnification for $M \leq 60$ kNm (**b**)

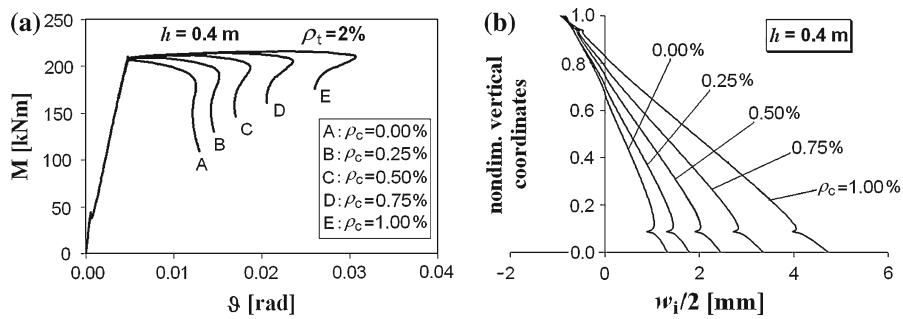

Fig. 9 Moment versus rotation diagrams (**a**), and nodal displacements (**b**), for different amounts of reinforcement in compression, ρ_c

also Carpinteri et al. 1989). However, this part of the diagram has a negligible effect on the overall behaviour of beams with reinforcement ratios higher than 0.25% (see Fig. 8b, where a magnification of Fig. 8a for $M \leq 60$ kNm is provided).

4.3 Effect of the steel reinforcement in compression

With regard to the introduction of reinforcement in compression, it determines a reduction in the compressed zone, particularly in the case of high tensile steel percentage. This reduction determines an increment in the crack opening displacement at the ultimate condition with a subsequent increment of the rotational capacity, as experimentally evidenced by Burns and Siess (1966). Numerical simulations have been carried out on RC beams with $h = 0.4$ m, $\rho_t = 2\%$, $\sigma_c = 40$ MPa, $\mathcal{G}_C = 30$ N/mm, $\sigma_u = 4$ MPa and $\mathcal{G}_F = 0.08$ N/mm. As shown in Fig. 9a, the ultimate rotation turns out to be an increasing function of the compression reinforcement percentage, ρ_c, which has been varied from 0 up to 1%. This trend can be clearly deduced by the displacement profiles of the points along the vertical cross-section shown in Fig. 9b. It is worth noting that the neutral axis depth considerably decreases by increasing the compression steel percentage, whereas the maximum interpenetration remains almost constant.

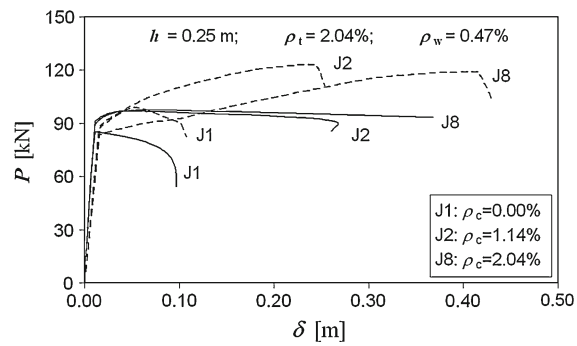

Fig. 10 Effect of the reinforcement in compression: numerical (*solid lines*) versus experimental (*dashed lines*) load-deflection curves. Experimental data are from Burns and Siess (1966)

A numerical–experimental comparison to assess the reliability of the model predictions is proposed in Fig. 10. The experimental data are from Burns and Siess (1966) and refer to RC beams with $h = 0.25$ m, $\rho_t = 2.04\%$, $\rho_w = 0.47\%$, and different values of ρ_c. The moment-rotation diagrams obtained from the numerical method are converted a posteriori into load-displacement curves for a direct comparison with experiments. A good agreement in terms of ultimate rotation is noticed, whereas the numeri-

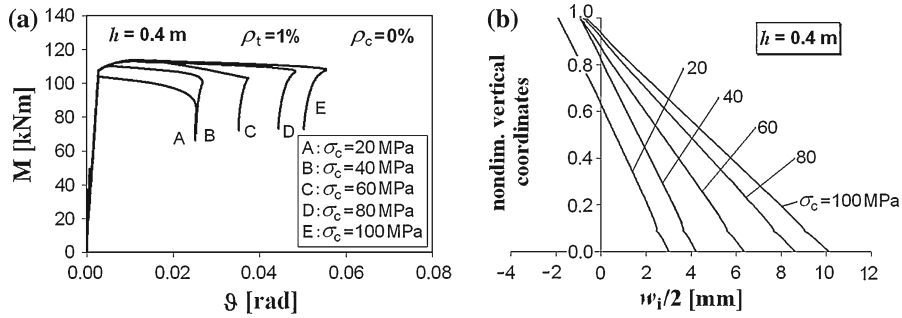

Fig. 11 Moment versus rotation diagrams (**a**), and nodal displacements (**b**) for different concrete compressive strengths, σ_c

Table 1 Overlapping law parameters for different concrete compressive strengths, σ_c

σ_c (MPa)	$\mathcal{G}_C$ (N/mm)	σ_u (MPa)	$\mathcal{G}_F$ (N/mm)
20	30.0	1.6	0.049
40	30.0	3.0	0.080
60	40.8	4.1	0.105
80	50.6	4.6	0.130
100	56.5	5.0	0.148

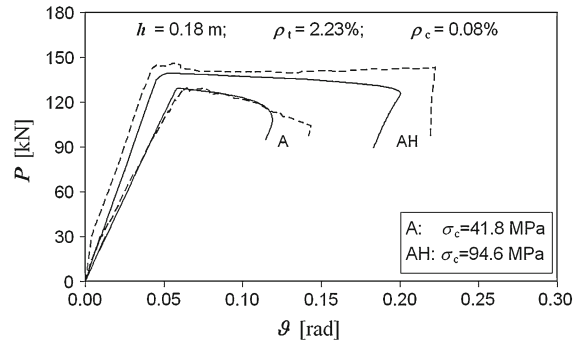

Fig. 12 Effect of the concrete compressive strength: numerical (*solid lines*) versus experimental (*dashed lines*) load-rotation diagrams. The experimental data are from Pecce and Fabbrocino (1999)

cal results underestimate the maximum load carrying capacity. This has to be ascribed to the actual hardening behaviour of steel which has not been modelled in the present study.

4.4 Effect of the concrete compressive strength

The rotational capacity is also an increasing function of the concrete compressive strength (see the experimental results from Pecce and Fabbrocino 1999; Shin et al. 1989; Markeset 1993). Analogously to the influence of the reinforcement in compression, in fact, the increment of the compressive strength determines a reduction in the crushing zone and a correspondent increment in the crack opening displacement. In order to investigate on the influence of such a parameter, the numerical simulations whose results are shown in Fig. 11 have been carried out by varying the compressive strength from 20 to 100 MPa, and computing $\mathcal{G}_C$ by means of Eq. (4) and σ_u and $\mathcal{G}_F$ according to the prescriptions in Model Code 90 (Comité Euro-International du Béton 1993) (see Table 1).

A numerical–experimental comparison is proposed in Fig. 12. The experimental data are from Pecce and Fabbrocino (1999) and refer to RC beams with $h = 0.18$ m, $\rho_t = 2.23\%$, $\rho_w = 0.25\%$, $\rho_c = 0.08\%$ and two different values of σ_c. The moment-rotation diagrams obtained from the numerical method are converted a posteriori into load-rotation curves for a direct comparison with experiments. A good agreement has to be noticed both for the ultimate rotation and the maximum load carrying capacity.

4.5 Effect of the stirrups confinement

Finally, the effect of the transversal reinforcement, usually introduced in RC beams in order to prevent shear failure, is investigated. The presence of stirrups, in fact, also influences the ductility, since it increases the concrete confinement, with a consequent increment in the compressive strength and the ultimate strain (see the experimental results from Burns and Siess 1966; Somes 1966; Shin et al. 1989). In the proposed model, this effect is taken into account by varying the crushing energy, and consequently the critical value of the overlapping displacement, according to Eq. (3). The values used in the numerical simulations are reported

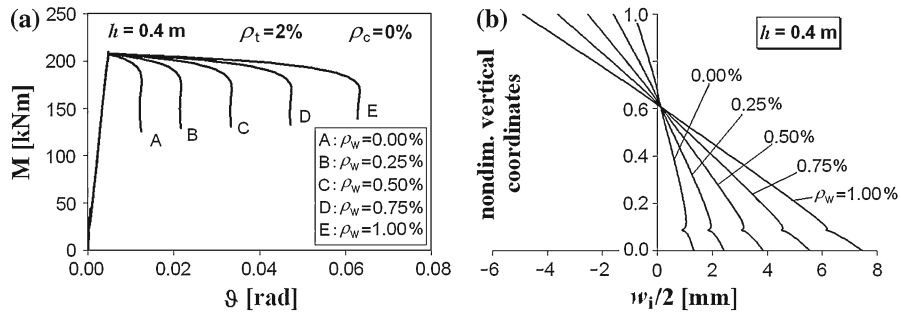

Fig. 13 Moment versus rotation diagrams (**a**), and nodal displacements (**b**) for different stirrups contents, ρ_w

Table 2 Overlapping law parameters for different stirrups contents, ρ_w

ρ_w (%)	σ_c (MPa)	$\mathcal{G}_C$ (N/mm)	w_{cr}^c (mm)
0.00	40.0	30.00	1.5
0.25	40.0	51.96	2.6
0.50	40.0	79.73	4.0
0.75	40.0	112.49	5.6
1.00	40.0	149.74	7.5

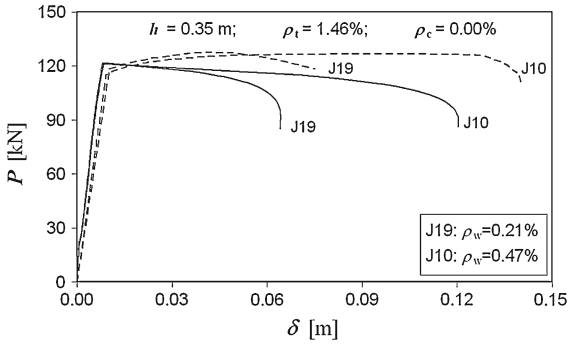

Fig. 14 Effect of the stirrups content: numerical (*solid lines*) versus experimental (*dashed lines*) load-deflection diagrams. The experimental data are from Burns and Siess (1966)

in Table 2. The numerical results are shown in Fig. 13a and confirm that the available ductility considerably increases by varying the stirrups percentage from 0 to 1%. The nodal displacement diagrams shown in Fig. 13b evidence the corresponding increment of the critical value of the crushing interpenetration.

A numerical–experimental comparison is proposed in Fig. 14. The experimental data are from Burns and Siess (1966) and refer to RC beams with $h = 0.35$ m, $\rho_t = 1.46\%$, $\rho_c = 0.00\%$ and two different values of ρ_w. The moment-rotation diagrams obtained from the numerical method are converted a posteriori into load-displacement curves for a direct comparison with experiments. Again, a good agreement has to be noticed for the predicted ultimate rotations.

5 Discussion and conclusions

Differently from the limit analysis, which yields only the ultimate load, the proposed model is able to investigate on size-scale effects, instability phenomena and ductile-to-brittle transitions in the mechanical response of RC beams. In particular, the softening behaviour in the increasing branch of the moment versus rotation diagram due to the cohesive contribution of concrete in tension can be captured, as well the softening (or snap-back) behaviour due to concrete crushing, as clearly evidenced in Figs. 6, 7, 8, 9, 10, 11, 12, 13 and 14. In all of these cases, the virtual snap-back branches are captured by governing the simulations with the crack and the crushing lengths as the driving parameters, rather than the applied load or the beam rotation.

A systematic application of the numerical algorithm by varying the main model parameters permits to correctly describe most of the experimental tests carried out in the last decades to investigate on the rotational capacity of RC beams (Burns and Siess 1966; Corley 1966; Somes 1966; Shin et al. 1989; Markeset 1993; Bosco and Debernardi 1993; Bigaj and Walraven 1993; Pecce and Fabbrocino 1999). In particular, we can conclude that the available ductility is an increasing function of the compression steel percentages, the concrete compressive strength, the stirrups contents, whereas it decreases as the tensile steel percentage and/or the structural dimension increase.

It is worth noting that the assumption of linear constitutive relationships, as well as the use of linear-elastic finite elements, permits to correctly describe very complex phenomena by means of simple calculations. Furthermore, the proposed model can be easily extended

to characterise the mechanical behaviour of fibre-reinforced structural elements (Cotterell et al. 1992; Li and Liang 1986; Wecharatana and Shah 1983; Visalvanich and Naaman 1983). The increment of the matrix toughness due to the presence of fibres in concrete, in fact, may be globally considered by modifying the cohesive law. On the other hand, the analysis of deep RC beams characterized by reinforcements distributed over the whole web may be carried out by considering multiple reinforcement levels in tension. The introduction of an axial force in addition to the applied bending moment will also permit to study the mechanical behaviour of eccentric axial loading elements, as, for example, columns and pre-stressed beams.

Acknowledgments The Authors would like to acknowledge the financial support of the European Union to the Leonardo da Vinci Project "Innovative Learning and Training on Fracture (ILTOF)", where Prof. Carpinteri and Dr. Paggi are involved, respectively, as the Project Coordinator and the Scientific Secretary.

References

Barbosa AF, Ribeiro GO (1998) Analysis of reinforced concrete structures using ANSYS nonlinear concrete model. In: Idelsohn S, Onate E, Dvorkin E (eds) Computational mechanics: new trends and applications, pp 1–7

Bigaj A, Walraven JC (1993) Size effect on rotational capacity of plastic hinges in reinforced concrete beams. CEB Bull Inf 218:7–23

Bosco C, Carpinteri A (1991) Softening and snap-through behaviour of reinforced elements. ASCE J Eng Mech 118:1564–1577

Bosco C, Debernardi PG (1993) Influence of some basic parameters on the plastic rotation of reinforced concrete elements. CEB Bull Inf 218:25–44

Burns NH, Siess CP (1966) Plastic hinging in reinforced concrete. ASCE J Struct Div 92:ST–5:45–61

Carpinteri A (1984) Stability of fracturing process in RC beams. ASCE J Struct Eng 110:544–558

Carpinteri A (1985) Interpretation of the Griffith instability as a bifurcation of the global equilibrium. In: Shah SP (ed) Application of fracture mechanics to cementitious composites. Martinus Nijhoff, Dordrecht pp 287–316

Carpinteri A (1989) Size effects on strength, toughness, and ductility. ASCE J Eng Mech 115:1375–1392

Carpinteri A, Massabò R (1997) Continuous vs discontinuous bridged-crack model for fibre-reinforced materials in flexure. Int J Solids Struct 34:2321–2338

Carpinteri A, Corrado M (2009) An extended (fractal) Overlapping Crack Model to describe crushing size-scale effects in compression. Eng Fail Anal 16:2530–2540

Carpinteri A, Colombo G, Ferrara G, Giuseppetti G (1989) Numerical simulation of concrete fracture through a bilinear softening stress-crack opening displacement law. In: Shah SP, Swartz SE (eds) Proceedings of SEM-RILEM international conference on fracture of concrete and rock. Houston, Texas, pp 131–141

Carpinteri A, Ciola F, Pugno N, Ferrara G, Gobbi ME (2001) Size-scale and slenderness influence on the compressive strain-softening behaviour of concrete. Fatigue Fract Eng Mater Struct 24:441–450

Carpinteri A, Ferro G, Ventura G (2004) Double brittle-to-ductile transition in bending of fibre reinforced concrete beams with rebars. Int J Numer Anal Meth Geomech 28:737–756

Carpinteri A, Ventura G, Carmona JR (2007a) Flexural to shear and crushing failure transitions in RC beams by the Bridged Crack Model. In: Carpinteri A, Gambarova P, Ferro G, Plizzari G (eds) Fracture mechanics of concrete structures, Proc. of FraMCoS-6, vol 2. Taylor & Francis, London, pp 677–684

Carpinteri A, Corrado M, Paggi M, Mancini G (2007b) Cohesive versus Overlapping Crack Model for a size effect analysis of RC elements in bending. In: Carpinteri A, Gambarova P, Ferro G, Plizzari G (eds) Fracture mechanics of concrete structures, Proc. of FraMCoS-6, vol 2. Taylor & Francis, London, pp 655–663

Carpinteri A, Paggi M, Zavarise G (2008) The effect of contact on the decohesion of laminated beams with multiple microcracks. Int J Solids Struct 45:129–143

Carpinteri A, Corrado M, Mancini G, Paggi M (2009) The overlapping crack model for uniaxial and eccentric concrete compression tests. Mag Concr Res 61:745–757

Carpinteri A, Corrado M, Paggi M (2010) An analytical model based on strain localization for the study of size-scale and slenderness effects in uniaxial compression tests. Strain. doi:10.1111/j.1475-1305.2009.00715.x

Cela JJL (2002) Material identification procedure for elastoplastic Drucker–Prager model. ASCE J Eng Mech 128:586–591

Cervenka J, Papanikolaou VK (2008) Three dimensional combined fracture-plastic material model for concrete. Int J Plast 24:2192–2220

Comité Euro-International du Béton (1993) CEB-FIP model code 1990, Thomas Telford Ltd, Lausanne. CEB Bull Inform 213/214

Corley GW (1966) Rotational capacity of reinforced concrete beams. J Struct Div 92:121–146

Cotterell B, Paravarivam P, Lam KY (1992) Modelling the fracture of cementitious composites. RILEM Mater Struct 25:14–20

De Borst R (1986) Non-linear analysis of frictional materials. Ph.D. Thesis, Delft University of Technology, The Netherlands

Fantilli AP, Iori I, Vallini P (2007) Size effect of compressed concrete in four point bending RC beams. Eng Fract Mech 74:97–108

Ferro G, Carpinteri A (2008) Effect of specimen size on the dissipated energy density in compression. J Appl Mech 75:41003/1–41003/8

Grassl P, Jiràsek M (2006) Damage-plastic model for concrete failure. Int J Solids Struct 43:7166–7196

Hillerborg A, Modeer M, Petersson PE (1976) Analysis of crack formation and crack growth in concrete by means of fracture mechanics and finite elements. Cement Concr Res 6: 773–782

Jansen DC, Shah SP (1997) Effect of length on compressive strain softening of concrete. ASCE J Eng Mech 123: 25–35

Kotsovos MD (1983) Effect of testing techniques on the post-ultimate behaviour of concrete in compression. RILEM Mater Struct 16:3–12

Li VC, Liang E (1986) Fracture processes in concrete and fiber reinforced cementitious composites. ASCE J Eng Mech 112:566–586

Markeset G (1993) Failure of concrete under compressive strain gradients. Ph.D. Thesis, The Norwegian Institute of Technology, Trondheim

Menétrey P, Willam KJ (1995) Triaxial failure criterion for concrete and its generalization. ACI Struct J 92:311–318

Morley CT (2008) When plasticity?. Mag Concr Res 60: 561–568

Owen DRJ, Hinton E (1980) Finite elements in plasticity, theory and practice. Pineridge, Swansea

Owen JM, Figueiras JA, Damjanic F (1983) Finite element analysis of reinforced and prestressed concrete structures including thermal loading. Comput Methods Appl Mech Eng 41:323–366

Papanikolaou VK, Kappos AJ (2007) Confinement-sensitive plasticity constitutive model for concrete in triaxial compression. Int J Solids Struct 44:7021–7048

Pecce M, Fabbrocino G (1999) Plastic rotation capacity of beams in normal and high-performance concrete. ACI Struct J 96:290–296

Pramono E, Willam KJ (1989) Fracture energy-based plasticity formulation of plain concrete. ASCE J Eng Mech 115: 1183–1204

RILEM TC 148-SSC (1997) Strain-softening of concrete in uniaxial compression. RILEM Mater Struct 30:195–209

Ruiz G, Elices M, Planas J (1999) Size effect and bond-slip dependence of lightly reinforced concrete beams. In: Carpinteri A (ed) Minimum reinforcement in concrete members. Elsevier, Oxford pp 67–98

Shin S, Ghosh SK, Moreno J (1989) Flexural ductility of ultra-high-strength concrete members. ACI Struct J 86:394–400

Simo JC, Ju JW (1987) Strain and stress-based continuum damage models: I formulation, II computational aspects. Int J Solids Struct 23:821–869

Somes NF (1966) Technical report: moment-rotation characteristics of prestressed concrete members, stage I: rectangular sections, TRA/398. Cement and Concrete Association, London

Suzuki M, Akiyama M, Matsuzaki H, Dang TH (2006) Concentric loading test of RC columns with normal- and high-strength materials and averaged stress–strain model for confined concrete considering compressive fracture energy. In: Proceedings of the 2nd fib Congress, Naples, Italy, cd-rom ID 3–13

van Mier J (1984) Strain softening of concrete under multiaxial compression. Ph.D. Thesis, Eindhoven University of Technology, The Netherlands

Visalvanich K, Naaman AE (1983) Fracture model for fiber reinforced concrete. ACI J 80:128–138

Wecharatana M, Shah SP (1983) A model for prediction of fracture resistance of fiber reinforced concrete. Cement Concr Res 13:819–829

Williams J, Hadavinia H (2002) Analytical solutions for cohesive zone models. J Mech Phys Solids 50:809–825